Multifunctional Core–Shell Nanoparticles as Highly Efficient Imaging and Photosensitizing Agents

ARTICLE *in* LANGMUIR · AUGUST 2009

Impact Factor: 4.46 · DOI: 10.1021/la902235d · Source: PubMed

Langmuir
Article
pubs.acs.org/Langmuir

Multifunctional Core−Shell Nanoparticles as Highly Efficient Imaging and Photosensitizing Agents

Ruirui Zhang,[†,‡] Chuanliu Wu,[†] Lili Tong,[‡] Bo Tang,*[,‡] and Qing-Hua Xu*[,†]

[†]*Department of Chemistry, National University of Singapore, Singapore 117543, Singapore, and* [‡]*College of Chemistry, Chemical Engineering and Materials Science, Shandong Normal University, Jinan 250014, P. R. China*

Received March 17, 2009

Here we report the preparation of a novel multifunctional core−shell nanocomposite material that contains a nonporous dye-doped silica core and a mesoporous silica shell containing photosensitizer molecules, hematoporphyrin (HP). This architecture allows simultaneous fluorescence imaging and photosensitization treatment. The photosensitizer molecules are covalently linked to the mesoporous silica shell and exhibit excellent photo-oxidation efficiency. The efficiency of photo-oxidation of the core−shell hybrid nanoparticles was demonstrated to be significantly improved over that in the homogeneous solution. The mesoporous silica nanovehicle acts not only as a carrier for the photosensitizers but also as a nanoreactor to facilitate the photo-oxidation reaction. The doping of fluorescence dyes into the nonporous core endows the imaging capability, which has been demonstrated with cell imaging experiments. This approach could be easily extended to conjugate other functional regents if necessary. These multifunctional nanovehicles possess unique advantages in acting as nanocarriers in photodynamic therapy to allow simultaneous high-resolution targeting and treatment.

Introduction

Multifunctional nanomaterials have important implications in biological studies from cellular to the integrative level owing to their capability of providing a robust framework for incorporating diverse functionalities.[1−4] Several types of hybrid nanomaterials with two or more capabilities of imaging, targeting, drug delivery, and therapy have been developed.[1−13] Among various multifunctional materials, silica nanoparticles were promising candidates as platforms to assemble versatile reagents, which not only allow multiple functions to be brought together but also improve the biocompatibility and alleviate the cytotoxicity.[10−13]

Photosensitizers have been wildly used in cell biology, photodynamic therapy (PDT), and blood sterilization.[14−20] In a PDT process, absorption of light will promote the photosensitizer molecules onto the excited state, which subsequently undergo intersystem crossing to the triplet state and then transfer the energy to ground state oxygen to initiate the generation of cytotoxic species, such as singlet oxygen ($^1O_2$) and other reactive oxygen species (ROS). These cytotoxic species will oxidize biomolecules and cause cell death eventually. The oxidative damage mainly depends on the quantum yields of $^1O_2$ and the efficiency of the subsequent photo-oxidation reaction, which are two basic assessment criteria in designing photosensitizers. Many different strategies have been proposed to improve photosensitizing capability. Fullerenes and their derivatives have been known to display high quantum yields of $^1O_2$ generation.[21] The major disadvantage of fullerenes is their absorption properties. Their absorption spectrum is highest in the UVA and blue regions of the spectrum where the tissue penetration depth of illumination is short, and the tail of absorption does not stretch out into the red regions (> 600 nm). In addition, they are not amenable molecules for drug delivery, and choosing appropriate formulations may be difficult. Metal nanoparticle bound photosensitizers have been reported to exhibit a remarkable enhancement of the quantum yield of singlet oxygen generation.[22] One potential problem is that metal nanoparticles might induce nonspecific binding interactions

*Corresponding authors: e-mail tangb@sdnu.edu.cn (B.T.), chmxqh@nus.edu.sg (Q.-H.X.); Fax +65 6779 1691.

(1) Jiang, W.; Kim, B. Y. S.; Rutka, J. T.; Chan, W. C. W. *Nat. Nanotechnol.* **2008**, *3*, 145–150.
(2) Jaiswal, J. K.; Simon, S. M. *Nat. Chem. Biol.* **2007**, *3*, 92–98.
(3) Michalet, X.; Pinaud, F. F.; Bentolila, L. A.; Tsay, J. M.; Doose, S.; Li, J. J.; Sundaresan, G.; Wu, A. M.; Gambhir, S. S.; Weiss, S. *Science* **2005**, *307*, 538–544.
(4) Wang, L.; Zhao, W.; Tan, W. *Nano Res.* **2008**, *1*, 99–115.
(5) Burns, A.; Ow, H.; Wiesner, U. *Chem. Soc. Rev.* **2006**, *35*, 1028–1042.
(6) Bechet, D.; Couleaud, P.; Frochot, C.; Viriot, M.; Guillemin, F.; Barberi-Heyob, M. *Trends Biotechnol.* **2008**, *26*, 612–621.
(7) Liong, M.; Lu, J.; Kovochich, M.; Xia, T.; Ruehm, S. G.; Nel, A. E.; Tamanoi, F.; Zink, J. I. *ACS Nano* **2008**, *2*, 889–896.
(8) Kim, J.; Kim, H. S.; Lee, N.; Kim, T.; Kim, H.; Yu, T.; Song, I. C.; Moon, W. K.; Hyeon, T. *Angew. Chem., Int. Ed.* **2008**, *47*, 8438–8441.
(9) Tada, D. B.; Vono, L. L. R.; Duarte, E. L.; Itri, R.; Kiyohara, P. K.; Baptista, M. S.; Rossi, L. M. *Langmuir* **2007**, *23*, 8194–8199.
(10) Jin, Y.; Kannan, S.; Wu, M.; Zhao, J. X. *Chem. Res. Toxicol.* **2007**, *20*, 1126–1133.
(11) Bakalova, R.; Zhelev, Z.; Aoki, I.; Masamoto, K.; Mileva, M.; Obata, T.; Higuchi, M.; Gadjeva, V.; Kanno, I. *Bioconjugate Chem.* **2008**, *19*, 1135–1142.
(12) Zou, H.; Wu, S.; Shen, J. *Chem. Rev.* **2008**, *108*, 3893–3957.
(13) Piao, Y.; Burns, A.; Kim, J.; Wiesner, U.; Hyeon, T. *Adv. Funct. Mater.* **2008**, *18*, 1–14.
(14) Macdonald, I. J.; Dougherty, T. J. *J. Porphyrins Phthalocyanines* **2001**, *5*, 105–129.
(15) Wilson, B. C.; Patterson, M. S. *Phys. Med. Biol.* **2008**, *53*, R61–R109.
(16) Castano, A. P.; Mroz, P.; Hamblin, M. R. *Nat. Rev. Cancer* **2006**, *6*, 535–545.
(17) Hamblin, M. R.; Hasan, T. *Photochem. Photobiol. Sci.* **2004**, *3*, 436–450.
(18) Collins, H. A.; Khurana, M.; Moriyama, E. H.; Mariampillai, A.; Dahlstedt, E.; Balaz, M.; Kuimova, M. K.; Drobizhev, M.; Yang, V. X. D.; Phillips, D.; Rebane, A.; Wilson, B. C.; Anderson, H. L. *Nat. Photonics* **2008**, *2*, 420–424.
(19) DeRosa, M. C.; Crutchley, R. *J. Coord. Chem. Rev.* **2002**, *233−234*, 351–371.
(20) Li, H.; Marotta, D. E.; Kim, S.; Busch, T. M.; Wileyto, E. P.; Zheng, G. *J. Biomed. Opt.* **2005**, *10*, 041203.
(21) Mroz, P.; Tegos, G. P.; Gali, H.; Wharton, T.; Sarnad, T.; Hamblin, M. R. *Photochem. Photobiol. Sci.* **2007**, *6*, 1139–1149.
(22) Wieder, M. E.; Hone, D. C.; Cook, M. J.; Handsley, M. M.; Gavrilovic, J.; Russell, D. A. *Photochem. Photobiol. Sci.* **2006**, *5*, 727–734.

with other biological molecules. Recently novel nanocomposites have been prepared by encapsulation of photosensitizers into nonporous silica nanoparticles for photodynamic therapy. However, the specific targeting properties of the photosensitizers might be lost after incorporation of these photosensitizer molecules into the nonporous silica.[21−24] Mesoporous silica nanoparticles possess large surface area and high accessible pore volume, which are very useful in drug delivery, adsorption and separation, molecular sensing, and catalysis.[25−30] Despite many advantages of their architectures, the application of mesoporous silica nanoparticles as photosensitizing vehicles has been rarely explored so far.

The precise localization of photosensitizers in cell or body is very important for the photosensitizing reaction or treatment. The use of photosensitizers requires great care to avoid nonspecific damage.[31] Incorporation of magnetic resonance contrast agents and photosensitizer molecules into a nanoparticle can offer dual capability of imaging and therapy, which renders more efficient and reliable photosensitization. Magnetic resonance imaging (MRI) offers the ability to follow the distribution of photosensitizer molecules in vivo, which can provide anatomic reference. However, MRI does not satisfy the requirement for microspace monitoring single cell analysis or vessel closure and thus cannot allow targeting with high spatial and temporal resolutions in living cells.[18] Compared to MRI, optical imaging methods can obtain detailed information at subcellular levels, which allow accurate targeting and simultaneous phototherapy treatment. Quantum dot−photosensitizer nanocomposites have been reported to have high singlet oxygen generation efficiency and could be used for fluorescence imaging in living organisms.[32−35] However, the application of quantum dot-based composites is hindered by their cytotoxicity, especially under photoirradiation. In addition, the photostability of quantum dot to $^1O_2$ is still under scrutiny.[32]

Here we report a highly efficient multifunctional nanocomposite material that contains a nonporous, dye-doped silica core for fluorescence imaging and a mesoporous silica shell containing photosensitizers (PS). This architecture allows simultaneous photosensitization treatment and fluorescence imaging. Fluorescein isothiocyanate (FITC) was chosen as the fluorescence imaging agent to be doped into the nonporous silica core, while the photosensitizer molecules, hematoporphyrin (HP), were covalently linked to the mesoporous silica. The nonporous silica core isolates the FITC dyes from the external environment and thus can help to protect the dyes from photobleaching.[36] The fluorescence imaging capability of these nanocomposites has been demonstrated with cellular experiments using HO-8910 PM cells. At the same time, the mesoporous shell allows O_2 diffuse in easily so as to interact with the photosensitizer molecules for ROS generation. The mesoporous silica shell provides a large pore volume for effective photosensitization. Furthermore, the photophysical properties and singlet oxygen generation capability of these nanocomposites could be engineered by varying the amount of FITC and HP molecules that are immobilized in the particle.

Experimental Section

Materials. Ammonium hydroxide (28−30%, J.T. Baker), tetraethoxysilane (TEOS) (98%, Fluka), 3-aminopropyltrimethoxysilane (APTS) (99%, Acros), fluorescein isothiocyanate (FITC) (90%, Fluka), hematoporphyrin (HP) (55%, Fluka), *N,N*-dicyclohexylcarbodiimide (DCC) (99%, Fluka), and 9,10-,10-anthracenediylbis(methylene)dimalonic acid (ABMD) (90%, Fluka) were used for the preparation of the nanoparticle samples. All other chemicals were from commercial sources and of analytical reagent grade, unless indicated otherwise. The highly metastasizing human ovarian cancer cell line (HO-8910 PM) was obtained from the Institute of Biochemistry and Cell Biology, Chinese Academy of Sciences, Shanghai, China. Water was purified with cartridges from Millipore (NANOPure, Barnstead) to a resistivity of 18.0 MΩ·cm.

Synthesis of Nonporous FITC@SiO_2 Cores. Silica nanoparticles were synthesized via a water-in-oil reverse microemulsion method.[37−39] APTS-FITC was prepared in advance. 0.1 mL of APTS was added into 2.5 mL of anhydrous ethanol solution containing 20.0 mg of FITC. The reaction proceeded for 24 h in the dark. The prepared precipitate was isolated by centrifugation and then dried in a desiccator for further use. The microemulsion consisted of a mixture of 5.3 mL of Triton X-100, 5.4 mL of *n*-hexanol, 22.5 mL of cyclohexane, 3.0 mg of APTS-FITC conjugates dissolved in 1.5 mL of deionized water, and 0.3 mL of ammonium hydroxide. The microemulsion was stirred for 30 min before 0.3 mL of TEOS was added. The solution was stirred for another 24 h. FITC-doped silica cores were isolated from the microemulsion by centrifugation at 14 000 rpm for 20 min and then washed with ethanol and deionized water for a few times. The obtained nanoparticles were dispersed in deionized water for further use.

Synthesis of HP-APTS Conjugates. DCC was used as the condensing agent to ensure that the carboxylic group of HP selectively reacts with the amino group of APTS in the presence of DMF. 3.3 mg of hematoporphyrin, 1.12 mg of DCC, and 10.0 μL of APTS were sequentially added into a 5.0 mL *N,N*-dimethylformamide (DMF) solution. The mixture was stirred overnight at room temperature. The obtained solution was directly used without further treatment.

Synthesis of HP-Conjugated Mesoporous Silica Nanoparticles. In a typical experiment, the prepared silica cores dispersed in water (0.3 mL) were added into a 10.0 mL 8 mM aqueous CTAB solution under stirring. 0.1 mL of 0.1 M NaOH solution was subsequently added. 30.0 μL of 20% TEOS in ethanol and 30 μL of as-prepared HP-APTS conjugates were injected into the above mixture three times at a 30 min interval. The reaction was allowed to further proceed for 24 h. The obtained nanoparticles were then centrifuged and washed with ethanol five times to remove the CTAB molecules. The obtained nanoparticles were dispersed in 1.5 mL of deionized water.

Photochemical Method To Monitor the Singlet Oxygen Generation. To assess the capability of $^1O_2$ generation of

(23) Ohulchanskyy, T. Y.; Roy, I.; Goswami, L. N.; Chen, Y.; Bergey, E. J.; Pandey, R. K.; Oseroff, A. R.; Prasad, P. N. *Nano Lett*. **2007**, *7*, 2835–2842.
(24) Yan, F.; kopelman, R. *Photochem. Photobiol*. **2003**, *78*, 587–591.
(25) Liu, R.; Zhao, X.; Wu, T.; Feng, P. *J. Am. Chem. Soc*. **2008**, *130*, 14418–14419.
(26) Feng, K.; Zhang, R.; Wu, L.; Tu, B.; Peng, M.; Zhang, L.; Zhao, D.; Tung, C. *J. Am. Chem. Soc*. **2006**, *128*, 14685–14690.
(27) Vallt-Regí, M.; Balas, F.; Arcos, D. *Angew. Chem., Int. Ed*. **2007**, *46*, 7548–7558.
(28) Slowing, I. I.; Trewyn, B. G.; Giri, S.; Lin, V. S.-Y. *Adv. Funct. Mater*. **2007**, *17*, 1225–1236.
(29) Wu, Y.; Cheng, G.; Katsov, K.; Sides, S. W.; Wang, J.; Tang, J.; Fredrickson, G. H.; Moskovits, M.; Stucky, G. D. *Nat. Mater*. **2004**, *3*, 816–822.
(30) Wang, J.; Tsung, C.; Hayward, R. C.; Wu, Y.; Stucky, G. D. *Angew. Chem., Int. Ed*. **2005**, *44*, 332–336.
(31) Kircher, M. F.; Mahmood, U.; King, R. S.; Weissleder, R.; Josephson, L. *Cancer Res*. **2003**, *63*, 8122–8125.
(32) Hardman, R. *Environ. Health Perspect*. **2006**, *114*, 165–172.
(33) Tsay, J. M.; Trzoss, M.; Shi, L.; Kong, X.; Selke, M.; Jung, M. E.; Weiss, S. *J. Am. Chem. Soc*. **2007**, *129*, 6865–6871.
(34) Shi, L.; Hernandez, B.; Selke, M. *J. Am. Chem. Soc*. **2006**, *128*, 6278–6279.
(35) Bakalova, R.; Ohba, H.; Zhelev, Z.; Ishikawa, M.; Baba, Y. *Nat. Biotechnol*. **2004**, *22*, 1360–1361.
(36) Zhao, X.; Bagwe, R. P.; Tan, W. *Adv. Mater*. **2004**, *16*, 173–176.
(37) Bagwe, R. P.; Hilliard, L. R.; Tan, W. *Langmuir* **2006**, *22*, 4357–4362.
(38) Bagwe, R. P.; Yang, C.; Hilliard, L. R.; Tan, W. *Langmuir* **2004**, *20*, 8336–8342.
(39) Wu, C.; Chen, C.; Lai, J.; Chen, J.; Mu, X.; Zheng, J.; Zhao, Y. *Chem. Commun*. **2008**, 2662–2664.

Scheme 1. Synthetic Procedure for Preparation of the Core−Shell Silica Nanoparticles and the Working Mechanism

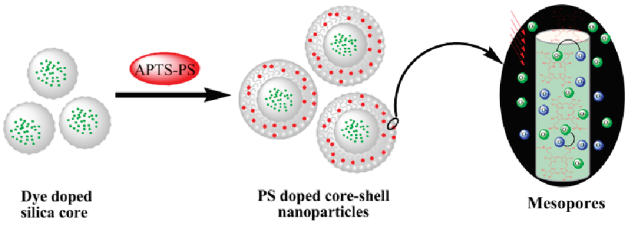

SiO_2@HP nanoparticles, disodium of 9,10-anthracenecliylbis-(methylene)dimalonic acid (ABMD) was employed as a probe molecule. ABMD molecules can react with singlet oxygen to yield an endoperoxide, which causes a decrease in the ABMD absorption around 400 nm.[40] Although the absorption spectrum of ABMD overlaps with that of HP, the ABMD absorption spectrum exhibits characteristic vibronic peaks at 360, 380, and 400 nm and can thus be distinctively discriminated. In the experiment, the proper amount of AMBD was added into the solution to be assessed; the singlet oxygen generation could thus be evaluated by monitoring the decrease of AMBD absorption under different irradiation periods.

Cell Culture and Imaging. The highly metastasizing human ovarian cancer cells were obtained by following protocols provided by the American type Tissue Culture Collection. Cells were seeded at a density of 1×10^6 cells mL^{-1} in RPMI 1640 medium supplemented with 10% fetal bovine serum (FBS), $NaHCO_3$ (2 g/L), and 1% antibiotics (penicillin/streptomycin, 100 U/mL). The cultures were maintained at 37 °C under a humidified atmosphere containing 5% CO_2. Florescence images were acquired on a LSM510 confocal laser-scanning microscope (Carl Zeiss Co., Ltd.) with an excitation wavelength of 488 nm.

Characterizations. High-resolution transmission electron microscopy (TEM) images of the nanoparticles were taken by using a JEOL JEM3010 field emission transmission electron microscope. One drop of the nanoparticle samples were placed onto the carbon-coated grids (150 meshes) and dried before loading into the TEM machine. The fluorescence and the UV−vis absorption spectra of the samples were measured by using a Perkin-Elmer LS55 luminescence spectrometer and a Shimadzu UV-2450 spectrophotometer, respectively.

Results and Discussion

The multifunctional nanoparticles were prepared by integrating a nonporous silica core with a mesoporous silica shell using a procedure as shown in Scheme 1. The as-prepared nonporous silica cores or dye-doped nonporous silica cores have a negatively charged surface.[12,37−39] A cationic surfactant, cetyltrimethylammonium bromide (CTAB), was used as an organic template for the formation of mesopores and to simultaneously provide nucleation sites for the growth of the silica shell. The HP molecules were covalently linked with 3-aminopropyltriethoxysilane (APTS) to form an APTS-HP conjugate in advance. After loading positively charged CTAB onto the silica cores, silica alkoxide precursor (tetraethyl orthosilicate, TEOS) and the APTS-HP conjugate were coinjected to form nanoparticles via a sol−gel co-condensation reaction.[8] The mesoporous core−shell nanoparticles were obtained after removing the CTAB templates by washing with ethanol.

Figure 1 shows the high-resolution TEM images of the typically obtained silica nanoparticles, which contain a solid nonporous core and a wormhole-like mesoporous shell. The HP

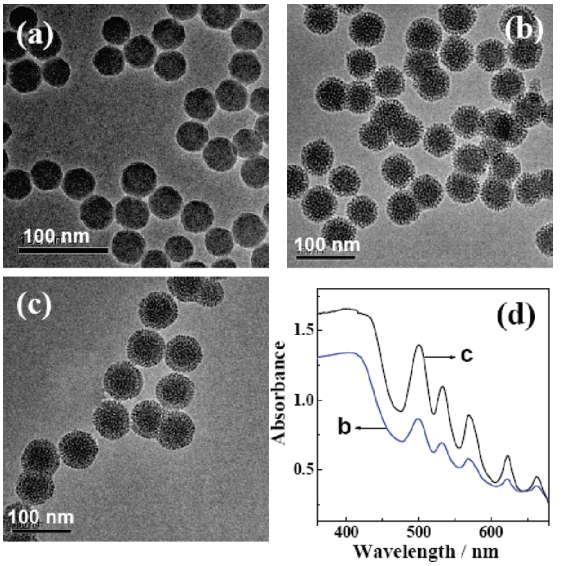

Figure 1. High-resolution TEM images of (a) silica cores, (b, c) mesoporous silica nanoparticles conjugated with different loading of HP molecules (SiO_2@HP), and (d) the absorption spectra of the SiO_2@HP nanoparticle samples shown in (b) and (c).

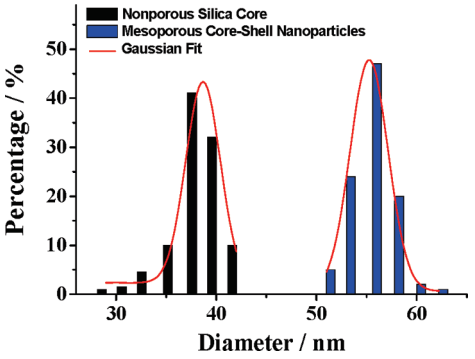

Figure 2. Histogram of the particles size distribution of the as-prepared samples.

molecules are conjugated with the mesoporous shell. The sizes of core−shell nanocomposites are quite uniform. Similar sized nanoparticles were obtained for different loading of HP molecules. Analysis of the TEM images revealed a monomodal particle size distribution with an average diameter of ~37 nm of silica cores and ~57 nm of mesoporous core−shell nanoparticles (Figure 2). These nanocomposites are very stable. They could be stored for over 1 month at room temperature without observation of any precipitation.

In a PDT process, absorption of light by photosensitizers eventually results in generation of singlet oxygen and other reactive oxygen species (ROS). Singlet oxygen is the major cytotoxic species that cause the cell death through the so-called type II mechanism.[14−19] To assess the capability of $^1O_2$ generation of SiO_2@HP nanoparticles, disodium of 9,10-anthracenecliylbis-(methylene)dimalonic acid (ABMD) was employed as a probe molecule. ABMD molecules can react with singlet oxygen to yield an endoperoxide, which causes a decrease in the ABMD absorption.[40] Although ABMD and the HP photosensitizers absorb in a similar spectral region (around 400 nm), the ABMD absorption spectrum exhibits characteristic vibronic peaks at 360, 380, and 400 nm and can thus be distinctively discriminated (the corresponding absorption spectra of HP and SiO_2@HP are given in the

(40) Lindig, B. A.; Rodgers, M. A. J.; Schaap, A. P. *J. Am. Chem. Soc.* **1980**, *102*, 5590–5593.

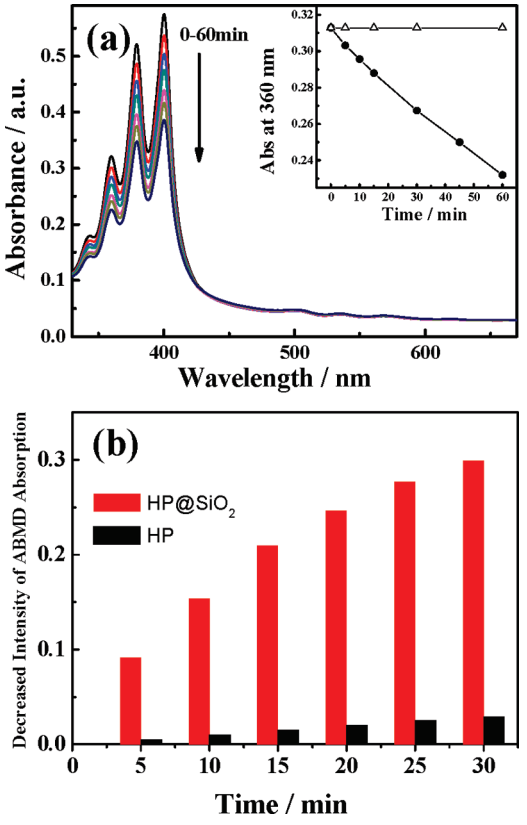

Figure 3. (a) Photo-oxidation of ABMD caused by singlet oxygen generated by the water dispersed HP-SiO_2 after different periods of irradiation with a 633 nm laser beam. Inset: absorption of ABMD at 360 nm as a function of irradiation time in the presence (solid circles) and absence (open triangles) of SiO_2@HP. (b) Time-dependent photo-oxidation of ABMD caused by singlet oxygen generated in water by using HP@SiO_2 nanoparticles and the same amount of HP in homogeneous solution.

Supporting Information). The photo-oxidation of ABMD was monitored for 1 h under the irradiation with a diode laser at 633 nm (Figure 3), a typical wavelength used in photodynamical therapy.[14] In the presence of SiO_2@HP, the ABMD absorption with distinct vibronic structures in the 350−420 nm range decreased continuously over the course of irradiation. In contrast, there is little change in the absorption of ABMD in the absence of SiO_2@HP (see Figure 3 inset), confirming that the photo-oxidation of ABMD is a result of a combined effect of SiO_2@HP and the light irradiation. It is also interesting to note that there is little change in the absorption at the longer wavelength range (430−650 nm) that arises solely from the HP molecules, suggesting that the HP molecules was not affected during the radiation. This result is consistent with the previously reported results that the covalently linked structure between HP and silica would increase the stability of photosensitizer.[41]

We have also done experiments to compare the photo-oxidation effect of the SiO_2@HP nanocomposites and the same amounts of HP molecules in homogeneous solution (Figure 3b). Intriguingly, the SiO_2@HP nanocomposites exhibit much higher efficiency in photo-oxidation of AMBD than that when the same amount of HP in homogeneous solution was used. The absorption of ABMD decreased dramatically under illumination at 633 nm in the presence of SiO_2@HP nanoparticles, about 10−15 times of that in the homogeneous solution. The results suggest

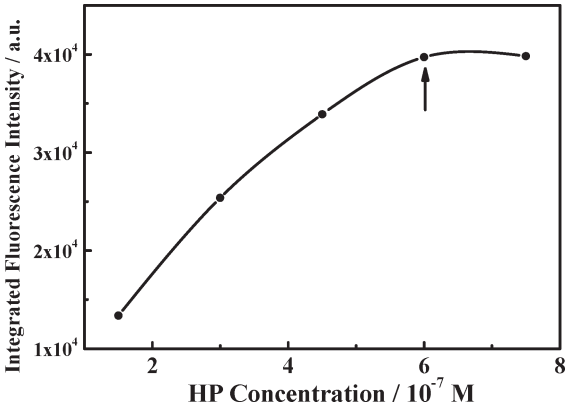

Figure 4. Integrated fluorescence intensity of SiO_2@HP versus different amount of HP loading.

that the mesoporous silica nanovehicles acted not only as a carrier for the photosensitizers but also as a nanoreactor to facilitate the photo-oxidation reaction.

In general, the process of the photosensitized oxidation involves three steps: (a) generation of $^1O_2$ by energy transfer from the triplet state of the photosensitizer to oxygen, (b) diffusion of $^1O_2$ to the reaction site, and (c) reaction of $^1O_2$ with the target molecules. In the SiO_2@HP core−shell nanoparticles, the photo-oxidation site is mainly located at the mesoporous channel inside the nanocomposites. The photosensitizer molecules (HP) are located in the nanocomposites, and thus the local concentration in the mesopore is higher than that in the homogeneous solution case, which results in more efficient $^1O_2$ generation. The mesoporous structure of the nanocomposites has high surface volume and can absorb the target molecules (ABMD here) into the mesoporous structure, thus enriching the local concentration of the ABMD. The photo-oxidation of the target molecules is thus more efficient. During the irradiation, the oxidized product, endoperoxide, is gradually generated and forms a concentration gradient between the mesoporous and solution phases, which act as a driving force for voluntary exchange of ABMD and the photo-oxidized product between two phases until the photo-oxidation reaction completes. Furthermore, in SiO_2@HP, both the $^1O_2$ generation and photo-oxidation occur in the mesoporous channel, which requires less diffusion time of $^1O_2$ before the photo-oxidation processes. Another factor is that the microenvironment of the silica mesopores will reduce the degree of freedom of the HP molecules. The HP molecules are bound to the mesopores that are comprised of totally inert silica matrix, a medium that is less reactive than water.[42] The singlet and triplet excited HP molecules are thus less likely being quenched or deactivated,[43] which will result in a longer excited state lifetime and enhanced $^1O_2$ generation efficiency. All these factors collectively contribute to a much higher photo-oxidation efficiency of the mesoporous materials compared to the homogeneous one.

It has to be noted that aggregation of HP molecules may deteriorate with the increasing amount of HP molecules incorporated into the nanoparticles. The aggregation of the HP molecules is manifested by the change in their emission spectra and saturation of emission intensity with increasing content of HP in the nanoparticles (Figure 4). For the sample indicated by arrow in Figure 4, it is estimated that around ~8000 HP molecules are

(41) Cantau, C.; Pigot, T.; Manoj, N.; Oliveros, E.; Lacombe, S. *ChemPhysChem* **2007**, *8*, 2344–2353.

(42) Chirvony, V.; Bolotin, V.; Matveeva, E.; Parhutik, V. *J. Photochem. Photobiol., A* **2006**, *181*, 106–113.

(43) Aebisher, D.; Azar, N. S.; Zamadar, M.; Gandra, N.; Gafney, H. D.; Gao, R.; Greer, A. *J. Phys. Chem. B* **2008**, *112*, 1913–1917.

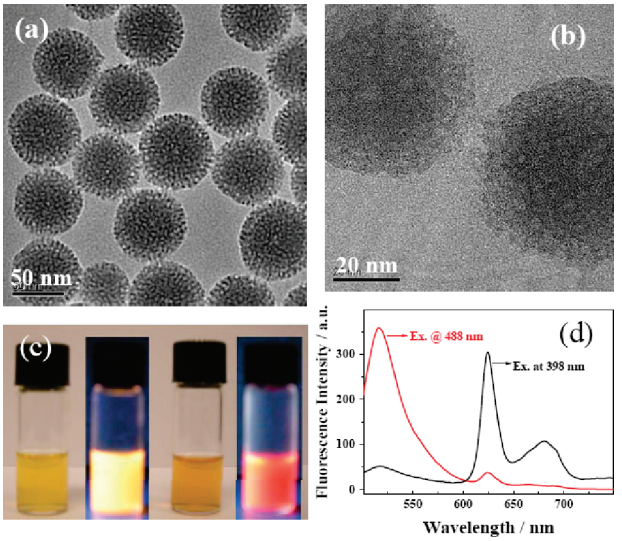

Figure 5. (a, b) HRTEM images of FITC@SiO_2@HP nanoparticles with different magnifications. (c) Picture of aqueous solutions of FITC@SiO_2@HP nanoparticles with different amounts of conjugated HP (~2000 and ~8000 HP molecules for two samples) and those under UV illumination. (d) Emission spectra of FITC@SiO_2@HP under excitation wavelength at 488 and 398 nm.

contained in a 60 nm silica nanoparticles, in which the aggregation was controlled to a reasonable level not to compromise the overall photosensitization efficiency.

One challenge in the multifunctional applications of mesoporous silica nanoparticles is how to endow the silica framework with effective, stable, and nonperturbative fluorescent probes. Conventional procedures based on covalent conjugation of fluorophores onto mesoporous surfaces or silica walls usually lead to poor fluorescence stability and unpredictable perturbations to the photosensitizer molecules. A core−shell nanocomposite with a nonporous silica core and a mesoporous shell can spatially separate fluorescence molecules (dye-doped core) from photosensitizer molecules (mesopore surface) as well as the external solution environments. We have prepared a core−shell nanocomposite, in which a fluorescein isothiocyanate (FITC)-doped nonporous silica core was coated with a mesoporous silica shell conjugated with HP (FITC@SiO_2@HP, Figure 5). HR-TEM images of the FITC@SiO_2@HP sample showed well-defined core−shell structures and a uniform size distribution. The TEM images with higher magnification (200 000×, Figure 5b) clearly shows that the shell of each individual nanoparticle is composed of mesopores with sizes of around 2−3 nm.

This core−shell nanocomposite material will have multifunction capability to allow simultaneous photosensitization treatment and fluorescence imaging. The loading of photosensitizer (HP) and fluorescent molecules (FITC) could be adjusted to tailor the applications. We have prepared core−shell nanocomposites with an identical FITC core but different loading of HP molecules. On the basis of the density of FITC-doped nanoparticles, it can be calculated that one nanoparticle contained about 6000 FITC molecules. For the two samples shown in Figure 5c, one FITC@SiO_2@HP nanoparticle contains ~2000 and ~8000 HP molecules, respectively. Under the illumination using a UV lamp, the FITC@SiO_2@HP mesoporous nanoparticles display different colors when the loading amount of the HP molecules was varied (Figure 5c). The FITC@SiO_2@HP nanoparticles dispersed in water exhibit different emissions under different excitation wavelengths. When excited at 488 nm (the absorption maximum of

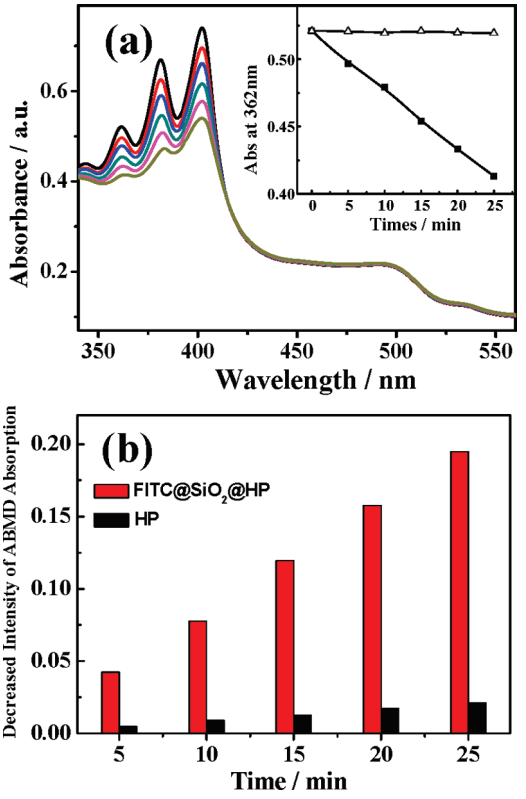

Figure 6. Photo-oxidation of ABMD caused by singlet oxygen generated by water dispersed FITC@SiO_2@HP after different irradiation time with a 633 nm laser beam. Inset shows absorption of ABMD at 360 nm as a function of irradiation time in the presence (solid squares) and absence (open triangles) of FITC@SiO_2@HP. (b) Time-dependent photo-oxidation of ABMD caused by singlet oxygen generated in water by using FITC@SiO_2@HP nanoparticles and the same amount of HP in homogeneous solution.

FITC), the nanoparticles (the sample with lower HP loading, ~2000 HP molecules per particle) showed a typical emission spectrum of FITC. While under excitation at 398 nm (the absorption maximum of HP), the emission spectrum is dominated by the emission of HP (Figure 5d).

The different emission spectra under different excitation wavelength suggest that these core−shell hybrid materials could be used for imaging and photosensitization by wavelength switch to allow light to be absorbed by FITC or HP selectively. Photosensitization is usually performed at 633 nm. Because FITC has no absorption at 633 nm, thus all of the light will be absorbed by the photosensitizer for photosensitization. Even if the photosensitization is performed at 398 nm, where FITC nearly have no absorption, the majority of the light will be absorbed by the photonsensitizers, and only a very small fraction of light will be absorbed by FITC, as evidenced by the emission spectra shown in Figure 5d. When excited at 398 nm, the emission intensity of FITC at 530 nm is only ~1/6 of the emission intensity of HP at 630 nm, despite the fact that the emission quantum yield of FITC is much larger than that of HP. For their applications in fluorescence imaging, a reasonable fraction of light needs to be absorbed by FITC. For the sample shown in Figure 6, although only ~45% of light is absorbed by FITC, the emission intensity is dominated by FITC due to much higher quantum yield of FITC compared to HP, as evidenced by the emission spectra shown in Figure 5b under excitation wavelength of 488 nm. The FITC loading in the core−shell nanoparticles could be adjusted to

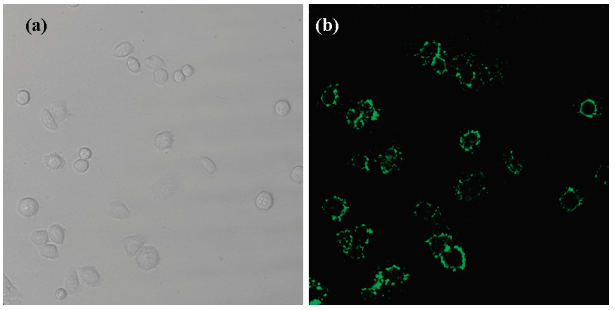

Figure 7. Bright-field (a) and fluorescence microscopy (b) images of the FITC@SiO_2@HP nanoparticles loaded HO-8910 PM cells. The images were taken after the FITC@SiO_2@HP nanoparticles were incubated with HO-8910 PM cells for 4 h on plate and then washed with phosphate buffered saline (PBS) to remove the non-internalized nanoparticles.

increase the fraction of light absorbed by FITC to tailor the particular applications.

The capability of singlet oxygen generation of FITC@SiO_2@HP has also been evaluated by photo-oxidation of AMBD under illumination at 633 nm (Figure 6). The results are similar to those of SiO_2@HP: the ABMD absorption band with distinct vibronic structures in the 350−420 nm range decreased continuously over the course of irradiation. On the other hand, the absorption spectra of the doped FITC molecules in silica core were not affected during the illumination processes, suggesting that FITC was not photo-oxidized by the singlet oxygen generation in the photosensitization processes owing to the protection from the nonporous silica wall. Similar to the results of SiO_2@HP nanoparticles (Figure 3b), the FITC@SiO_2@HP nanocomposites exhibit much higher efficiency in photo-oxidation of AMBD than that when the same amount of HP in homogeneous solution was used. Under illumination at 633 nm, the absorption of ABMD solution in the presence of SiO_2@HP nanoparticles decreased about 8−10 times faster than that in the homogeneous solution (Figure 6b).

We have also tested the fluorescence imaging capability of the FITC@SiO_2@HP nanoparticles by cell imaging experiments on the HO-8910 PM cells. Figure 7 shows the bright-field and fluorescent confocal microscopy images of the incubated cells. As can be seen from the images, the FITC@SiO_2@HP nanoparticles are mainly located at the surface of these cells, most likely the cell membrane, and a few were observed inside the cells.

In these core−shell hybrid nanoparticles, ~6000 FITC molecules are contained in a 60 nm core. The FITC might form aggregate to decrease the fluorescence efficiency. We have measured the fluorescence efficiencies and decay times of FITC in the silica shell and in homogeneous solutions. The data are shown in the Supporting Information (Figures S2 and S3). The emission intensity decreased about 45% after incorporation into the silica shell (Figure S2) due to aggregation effects, consistent with its fluorescence lifetime, which decreased from 2.1 to 1.1 ns (Figure S3). Considering the fact that there are ~6000 FITC molecules in one nanoparticle, the nanocomposite materials will display very strong fluorescence and can act as very bright fluorescence agents for fluorescence imaging.

Another potential problem is photostability of the fluorophores and photosensitizers. During the photosensitization processes, singlet oxygen is generated, which may damage the FITC and HP molecules.[44,45] The irradiation effects on the FITC fluorescence have also been tested and the results are shown in the Supporting Information (Figure S4). Upon irradiation at 633 nm (using the same laser source as used for photo-oxidation experiments) for 1 h, the emission intensity only decreased about 10%. The results demonstrated that the FITC inside the nonporous silica shell is well protected from the damage by singlet oxygen. The photostability of HP in silica matrix is demonstrated in the data shown in Figure 6. During the photo-oxidation process, the absorption spectra in the spectra range of 500−550 nm (which is solely due to the absorption of HP molecules) remained nearly unchanged under the 633 nm illumination for 30 min. At the same time, the photo-oxidation of AMBD proceeded linearly with time, suggesting that their singlet oxygen generation capability was not compromised. These results indicated that HP molecules in our nanocomposites have pretty good photostability.

In these FITC@SiO_2@HP core−shell nanaocomposites, their fluorescence capacity was achieved by doping the silica cores with FITC. In their potential applications, the FITC-doped core could be used as a "tracer", and photosensitizer loaded mesoporous silica shell could act as an "activator". These multifunctional nanoparticles could be also potentially utilized to trace the circulation of biomacromolecules (imaging and targeting), while performing photo-oxidation or photodynamic therapy treatment. This unique structure combines the advantages of nonporous and mesoporous silica materials and is superior to many conventional photosensitizing materials.[32−35]

Conclusions

In summary, we have used a simple procedure to prepare a novel multifunctional core−shell nanocomposite material with dual capability of fluorescence imaging and photosensitization. Cetyltrimethylammonium bromide (CTAB) was used as an organic template and simultaneously provided nucleation sites for the hydrolysis of silicane. The photosensitizer molecules are covalently linked to the mesoporous silica shell and exhibit excellent photo-oxidation efficiency. The efficiency of photo-oxidation of the core−shell hybrid nanoparticles was demonstrated to be significantly improved over that in the homogeneous solution. The mesoporous silica nanovehicle acts as not only as a carrier for the photosensitizers but also as a nanoreactor to facilitate the photo-oxidation reaction. The doping of fluorescence dyes into the nonporous core endows the imaging capability, which has been demonstrated with cell imaging experiments. This approach could be easily extended to conjugate other functional regents, such as Gd complexes, other fluorescence dyes, or recognition groups, if necessary. These multifunctional nanovehicles possess unique advantages in acting as nanocarriers for potential applications in photodynamic therapy to allow simultaneous high-resolution targeting and phototherapy treatment.

Acknowledgment. This work is supported by the Faculty of Science, National University of Singapore (R-143-000-341-112 and R-143-000-302-112). R. Zhang thanks the China Scholarship Council for scholarship support.

Supporting Information Available: Absorption spectra of HP@SiO_2 nanoparticles and HP (Figure S1), emission spectra of FITC and FITC-doped silica nanoparticles (Figure S2), fluorescence lifetime decay of FITC and FITC@SiO_2 (Figure S3), and fluorescence spectra of FITC@SiO_2@HP (Figure S4). This material is available free of charge via the Internet at http://pubs.acs.org.

(44) Kamat, P. V. *Chem. Rev.* **1993**, *93*, 267–300.
(45) Thomas, J. K. *Chem. Rev.* **1993**, *93*, 301–320.